The Non-Sphericity of Triton's Atmosphere as Evidenced by Stellar Occultations

by

Michael James Person

S.B. Physics (1994)

Massachusetts Institute of Technology

Submitted to the Department of Earth, Atmospheric, and Planetary Sciences
in Partial Fulfillment of the Requirements for the Degree of
Master of Science in Planetary Science

at the

Massachusetts Institute of Technology

May 2001

Signature of Author.....
.....
Michael James Person
Department of Earth, Atmospheric, and Planetary Sciences
May 11, 2001

Certified by .....
.....
James L Elliot
Professor of Physics and Planetary Science
Thesis Supervisor

Accepted by.....
Ronald G Prinn
Department of Earth, Atmospheric, and Planetary Sciences
Department Head

Abstract

In an attempt to reconcile and understand recent measurements of the non-sphericity in Triton's atmosphere, the Tr148 occultation data set was reanalyzed. Recent new data from the Hubble Space Telescope Fine Guidance System allowed the separation and position angle of the Tr148 double star to be independently incorporated into the occultation analysis rather than being freely fit during the occultation reduction. The separation of 0.3855 ± 0.0004 arcsec and position angle of 67.17 ± 0.05 deg determined here differ from the values determined solely from the occultation timings of 0.3874 ± 0.0011 arcsec and 65.16 ± 0.14 deg. This resulted in a change in the calculated ellipticity and position angle of Triton's half-light ellipse from their originally fitted values of 0.029 ± 0.016 and 70.3 ± 10.1 deg to improved values of 0.033 ± 0.013 and 65.1 ± 8.8 deg. By fixing the separation parameters to independently determined values instead of freely fitting for them, the confidence in the new ellipticity fit (as measure by the reduced chi-squared results) is significantly increased. This work ends with a discussion of these new values and their implications for Triton's atmosphere.

Contents

Table of Contents

List of Figures

List of Tables

Introduction

Since the Voyager 2 encounter with Triton, it has been clear that considerable activity occurs in Triton's atmosphere. Dust streaks on the surface imply significant winds at low altitude (Hansen, McEwen et al. 1990). Plumes are seen rising from the surface and being sheared off by higher altitude winds, drifting for over 100 km (Smith, Soderblom et al. 1989; Soderblom, Kieffer et al. 1990). Individual clouds were observed to move at the 8km level (Hansen, McEwen et al. 1990).

As Triton is one of the few bodies in the solar system in which the main atmospheric constituent (N_2) is present as a condensate on the surface, its atmospheric physics are governed by the vapor pressure equilibrium between the atmosphere and surface ices. This provides useful constraints that assist in determining the thermal structure of the atmosphere (Strobel, Zhu et al. 1996), and makes it an ideal candidate for atmospheric modeling (Spencer 1990). The Voyager encounter, while providing a wealth of data, that indicated continuing changes throughout the atmosphere, unfortunately provided only a single snapshot of the body: that of its state during the brief flyby. Any attempts to characterize trends, fit long-term models, or examine atmospheric evolution on Triton requires continual monitoring.

For small or distant solar system bodies there are few available means to make a detailed examination of atmospheric features of the body. For bodies such as Triton, which is both fairly small and very far away, the problem is even more difficult. In most cases, such continual monitoring is infeasible from the Earth, due to the tremendous resolution needed to resolve any features from such a large distance. There is one case where monitoring from Earth can provide the needed resolution, and that is the rare instance of stellar occultation. Stellar occultation events by bodies such as Triton provide a means of monitoring the body's atmosphere at various altitude levels directly from Earth because the measured starlight is diagnostic of the refractive characteristics of the specific levels of the atmosphere through which it passes (Baum and Code 1953; Elliot and Young 1992).

With a stellar occultation, it is possible to achieve resolution on the refractive properties of the atmosphere approaching the Fresnel diffraction limit (Baum and Code 1953). For the case of Triton (approximately 30 AU distant), occulting a star being observed in visible light (approximately 500 nm), the Fresnel limit is a mere 1.5 km.

In practice, there are further constraints on the actual resolution. Most notably is the integration time at which photometry of the incoming light can be acquired. For a typical Triton occultation with a shadow velocity of 25 km/sec and a high speed photometer operating at 5Hz will result in a maximum resolution of 5 km.

Other constraints may apply depending upon the specific situation. Chief among these is the signal to noise level available in the signal of the star being occulted (photon noise as well as any scintillation) but other effects need be considered as well, such as a finite resolvable diameter of the occultation star itself, but in general stellar occultations will always produce vastly finer spatial resolution when compared to any other earth based observing. This increased resolution and the direct probing of the atmosphere itself makes Earth based monitoring of the variable features of Triton's atmosphere discussed above possible.

One of the features of Triton's atmosphere well-suited to study by this method is the geometric figure. Over the five years from 1993 to 1997, four Triton occultations have been observed. The first of these, Tr60 (McDonald and Elliot 1992), was observed from only one station and not in the central flash region (discussed later) and therefore was not suitable for determining the atmospheric shape. The remaining three occultations, Tr148, Tr176, and Tr180 (McDonald and Elliot 1995) were all more extensively observed. All three occultations provide evidence that the atmosphere of Triton exhibits significant deviations from sphericity, but the measurements are not consistent with each other (Elliot, Stansberry et al. 1997; Olkin, Elliot et al. 1997; Elliot, Person et al. 2000).

This variable deviation from a sphere could be real and due to the ongoing activity described earlier. Indeed, frost migration models of Triton's atmosphere require significant relocation of nitrogen ice back and forth across the surface to maintain Triton's thermal balance

(Hansen and Paige 1992). Although the time scale of these oscillations is of the order of decades, short term variations associated with them could result in the changes seen.

In order to further characterize the stability of the non-sphericity of the atmosphere, this work will focus on Tr148, the occultation of a double star by Triton in August of 1995. The fact that Tr148 turned out to be a double star (not known until the event occurred) adds several difficulties to analysis which will be discussed in the following chapters.

Improvements to these previous Tr148 reductions will be made, with an eye towards increasing the confidence in the calculated ellipticity of the half-light surface. By adding an independent determination of the Tr148 double star system's separation and position angle, some of the ambiguities in the current results can be eliminated resulting in greater confidence fits to the solutions. These improved results will be compared to other measurements in an attempt to build a consistent picture of Triton's atmospheric figure, and increase confidence in the basic non-sphericity of the atmospheric structure.

Occultation Data Sets

Tr60, the first Triton occultation observed, was reduced by Olkin, Elliot et al. (1997) to yield measurements of the scale height and half-light radius of Triton's atmosphere. It was, however, only a single chord and thus, nothing could be said about the figure of the atmosphere from that event. The three remaining occultations available, Tr148, Tr176, and Tr180, provide several differing pictures of Triton's possible figure, though all three events indicate significant non-sphericity. What follows is an in-depth review of the Tr148 occultation and its results, with an eye towards searching for consistency as well as ways to improve the analysis. The analysis of the Tr176 event is also included for comparison.

Tr148 Astrometric Solution

On August 14, 1995, Triton occulted a 13th magnitude star designated Tr148 in the survey of McDonald and Elliot (1995) that first identified the possible event. The most widely observed Triton occultation ever, this event generated nine occultation light curves from stations around the globe, including data from the 0.9 m telescope of the Kuiper Airborne Observatory, the 3.0 m telescope from Hawaii's IRTF, a 1.8 meter telescope from Lowell Observatory, a pair of telescopes (0.9 m and 1.0 m) at Lick Observatory, and the 2.3 meter telescope at the Wyoming IR Observatory (WIRO). In 1997 Olkin, Elliot et al. (1997) compiled and used these disparate light curves to produce a single astrometric solution for the event.

The method used by Olkin, Elliot et al. (1997) was to individually establish the half-light times for immersion and emersion for each of the occultation chords by fitting models to individual light-curves in the manner of Elliot and Young (1992). These models improve over previous models (Baum and Code 1953) by including the variation of gravity with radius and limb focussing effects particular to small body occultations. They characterize the occultation light curve of a small body with an atmosphere in just a few parameters. The three parameters related to the absolute signal levels of the event are pre-occultation full signal level, background signal level

(minimum occultation light level), and a time-dependent slope in the background light if any, all measured in signal per second. The three parameters relating to the geometry of the event are occultation shadow velocity (v), time duration of a single integration (Δt), closest approach distance of the center of the shadow to the star location (ρ_{min}). Finally, three further parameters are sufficient to model the refractive properties of the atmosphere of the occulting body: the radius of the atmosphere at the half light level (r_h), the scale height at the half light level (H_h), and a thermal index (b), which is essentially an exponent to the power law specifying the radial thermal gradient of the atmosphere.

The (half-light) times of immersion and emersion can then be taken from the model by locating the two points where the model yields 50% of the occultation star's flux (including refractive and focussing effects). The strength of this method is that once these times are determined, it is no longer necessary to deal with the entire light curve data set. Using these half-light times alone, one can solve for the shape of the atmospheric surface of half light, that is, the atmospheric altitude at which the refracted light of the occulted star is reduced to one half of it's full value. Of course, it is the two-dimensional projection of this shape around the edge of the limb of the occulting body that is being fit for rather than the full three-dimensional surface itself. Hence, if the atmosphere is spherically symmetric, this figure of half-light in the fitting would be a circle as seen from the Earth.

To proceed, the coordinates of the various telescopes involved must be specified at each of the half-light times (a simple process for the ground based observers, though obviously more complicated for the KAO observations) and these, along with the ephemeris of Triton, converted to a common coordinate system for simultaneous plotting. This is most effectively done for this purpose by projecting onto a common f-g observer plane (with origin at the geocenter) in the manner of Elliot, Bosh et al. (1993).

The f and g axes lie in a plane perpendicular to the line between the center of the earth and the occultation star. All half-light points can be then projected onto this plane knowing only their geocentric coordinates, the celestial coordinates of the occultation star, and Triton's ephemeris. If

the center of Triton's figure is also projected onto this same plane over these same times, the differences between the location of each station in the plane at each half-light time can be plotted. Figure I shows such a plot, indicating the relative positions in the *f-g* plane of each of the immersion and emersion half-light points after subtracting the position of Triton's center for three of the Tr148 station. As seen, these points can be fit by a figure, centered on Triton, describing the shape of the half-light level of the atmosphere in two dimensional projection parallel to the direction of the occultation star. In the case of figure I, a circle was fit to these six points. Fitting is accomplished using the least squares minimization technique as described by Bevington (1969), minimizing the sum of squared residual perpendicular distances between each point and the modeled figure.

Figure I: Occultation Chords Plotted in *f-g* Space

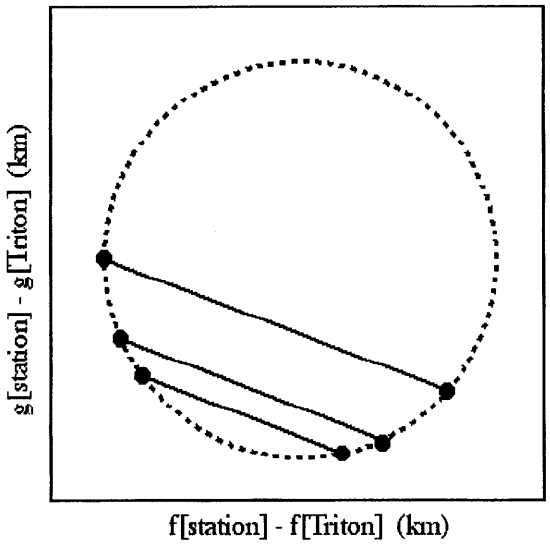

Figure I: *Occultation Geometry Plot* The solid lines connect the two half-light points of each occultation light curve. The end points of the three occultation chords shown above can be fit by a figure representing the two dimensional projection of the half-light surface of the atmosphere. In this case the dotted circle has been fit to those points.

Given the number of free parameters available when fitting, we see that three points, usually two occultation sites with an immersion and emersion chord from each (thus totaling four and allowing for data loss at one site), are required to constrain a circular atmospheric figure, while

at least five (usually three sites) are required for an ellipse. More complex figures would require more half-light points.

As an ellipse, or other non-circular figure, indicates a non-spherical shape in the atmosphere of the occulting body, examination of the residuals of such fits compared to those of circles should be sufficient to identify any non-sphericity in the atmosphere of the occulting body.

Unfortunately, as is often the case, this analysis is not so straight forward in practice. As all prior Earth-based observations were of insufficient resolution to detect this, the occultation observations themselves revealed that Tr148 was in fact an unsuspected double star (Olkin, Elliot et al. 1997). The two members of the pair, Tr148A and Tr148B, were each occulted by Triton separately and these occultations were variously visible from the observing stations. The team at Lick observatory was fortunate enough to record occultations of both members of the pair, revealing what had happened and providing an important geometric constraint for further analysis.

This double-star effect does not make analysis as described above impossible, merely more complex. Fortunately, it also increased the number of available timing chords, as Lick observatory observed both occultations. Proceeding as before, all recorded occultation curves can be plotted on a single plane provided those from the second star are shifted by an amount equal to the separation of the two stars. In that case, all half-light locations can once again be plotted on a single figure and allow fitting of a two-dimensional shape to the atmospheric half light profile. Figure II shows such a plot, taken from Olkin, Elliot et al. (1997), including all available Tr148 light curves. Note that Lick has two occultation chords on the figure, one from each component of the Tr148 double star.

Constructing such a figure and then fitting atmospheric profiles to the resulting points requires knowing the separation of the two stars constituents. Olkin, Elliot et al. (1997) resolved this issue by allowing the separation between the stars and the position angle of this separation to be two additional fitted parameters in the atmospheric figure fits. Given the relative wealth of data (six acceptable chords, thus twelve half-light points), adding two more free parameters is justified, though it does mean that on ellipical fits (with five free parameters needed to specify an ellipse and

two needed to specify the postion of Tr148B relative to Tr148A), there are just five degrees of freedom remaining out of the twelve data points.

Figure II: Tr148 Occultation Chords

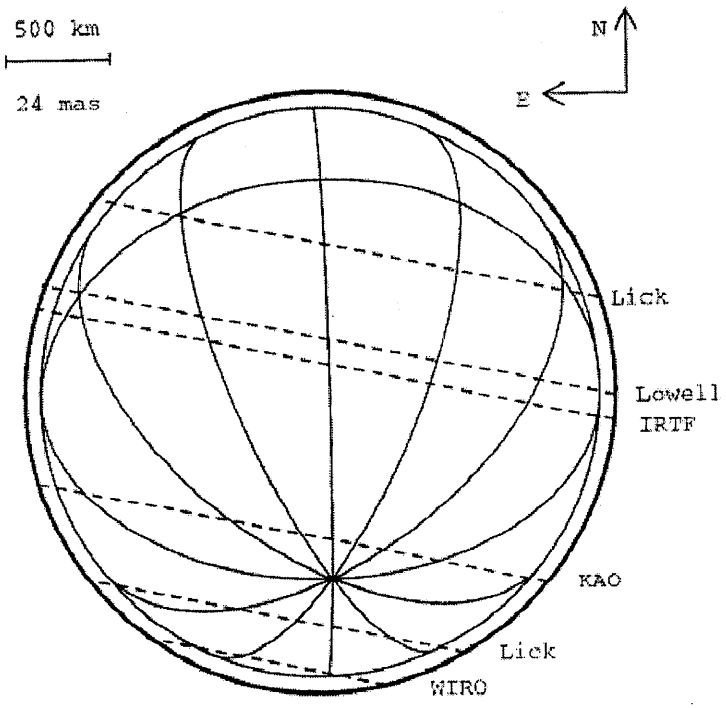

Figure II: *Tr148 occultation geometry.* Triton's globe as seen from the Earth during the Tr148 occultation. The lower three chords are occultations of the primary star Tr148A, and the upper three chords are occultations of the companion Tr148B. Also shown are the south pole with latitude lines radiating away. Note that Lick has two chords as both occultation events were recorded from that location. The large concentric circles are the half-light altitude of the atmosphere and Triton's surface. Adapted from Olkin, Elliot et al. (1997)

However, as will be seen in a later occultation (Tr176), five degrees of freedom is a relative luxury in this area, so reduction continued as described above with the new fits. Using these six chords, and leaving the separation and position angle of the double star as free parameters, Olkin, Elliot et al. (1997) adopted two solutions for the geometric figure of the projected half-light surface, one circular and one elliptical. These results are summarized in Table I.

Given the residuals of the fits and the change of the number of degrees for freedom between the two cases, the weighted RMS residual per degree of freedom for the two fits does

indicate that the elliptical fit is preferred, though not by enough to completely rule out the circular solution. The best elliptical fit resulted in a reduced chi-squared that would be expected for a correct model with probability 14%, while the best circular fit corresponded to a probability of 5%. Thus this data set alone can not well constrain any possible non-sphericity in the atmosphere of Triton at the time of the Tr148 occultations.

Table I: Atmospheric Figures from Tr148 Half-Light Analysis[a]

	Circular Fit	Elliptical Fit
Half-light Radius[b] (km)	1427.9 ± 3.5	1432.6 ± 5.7
Ellipticity	N/A	0.029 ± 0.016
Position Angle[c] (deg)	N/A	70.3 ± 10.1
Double Star Separation (arcsec)	0.3869 ± 0.0012	0.3874 ± 0.0011
Double Star Position Angle[d]	65.75 ± 0.16	65.16 ± 0.14
Sum of Squared Residuals (km)	1504	707
Weighted RMS residual	14.7	11.9
Reduced Chi-squared	2.1	1.7

[a] (Olkin, Elliot et al. 1997)

[b] For the elliptical fit, the semi-major axis is given in the shadow plane, which due to refraction by Triton's atmosphere, is one scale height smaller than the radius at which the starlight made its closest approach to Triton's center.

[c] Pole position of the semi-minor axis of atmospheric ellipse measured from North through East.

[d] Position angle of Tr148B with respect to Tr148A measured from North through East.

Note from Table I however, that the fitted error in the double star separation in each case is larger than the difference between the double star separations of both cases. This indicates that, given the methods of analysis used, a definitive value of the separation of the two components of the Tr148 double star found independently of the figure fitting, might differentiate between the elliptical and circular fits. This hypothesis will be examined in the following chapter.

Tr148 Central Flash Solution

A second method of determining the ellipticity of the atmospheric figure involves only one light curve at a time, though that light curve must be very close to including the center of the shadow. Thus few chords permit this analysis. The method uses the central portion of the light curve, where intense focussing of light from around all limbs of the planet results in a spike in the signal in the middle of the weakest part of the occultation profile. This enhancement occurs only when the observer is very close to the center of Triton's shadow allowing focussed light to be concentrated from all around the body, and is thus called the "central flash".

For an occultation by a spherically symmetric body, (circular half-light figure), this central flash should be symmetric with respect to the center of the light curve no matter how the occultation geometry is set up. However, in the case that the half-light figure is not circular, focussing from closer and farther parts of the planet's limb results in a central flash that is not symmetric with respect to the light curve.

As can be seen in Figure II, the two closest stations to the center of the shadow during the Tr148 occultation were Tr148B occultations as seen from the IRTF and Lowell Observatory. Unfortunately, the Lowell Observatory data did not have sufficient signal to noise to properly resolve the increase in flux associated with the central flash if indeed it were visible there.

Both detectors at the IRTF however recorded the central flash. It was noted that the central flash was asymmetric with respect to the center of the light curve, in both cases occurring seconds after the midpoint between the two half light times. Figure III shows the asymmetry in the light curves, as evidenced by the delay in the central flash for the IRTF data.

Olkin, Elliot et al. (1997), recognizing this asymmetry, excluded the middle 20% of each light curve from their fitting when determining half-light times, and later while examining thermal parameters from their fits. Later that year, (Elliot, Stansberry et al. 1997) published an examination of the asymmetry including an improved fitting model that did not assume a circular focussing profile, but rather allowed ellipticity in the atmospheric half-light figure to produce an asymmetric central flash such as those observed from the IRTF (Elliot, Stansberry et al. 1997).

Figure III: Asymmetry in Tr148B IRTF Data

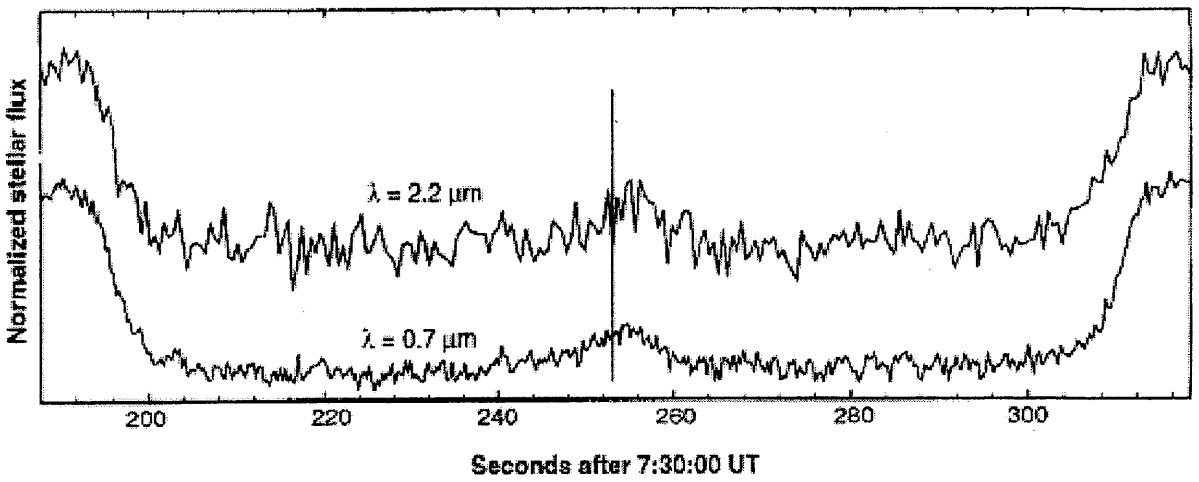

Figure III: *Tr148 IRTF data.* This plot shows both the IR and visible light curves from the Tr148 occultation as recorded at the IRTF. The vertical bar denotes the midpoint in time between the immersion and emersion half-light levels of the occultation. Note that the central flash (the increase in flux near the center of the event) is asymmetric with respect to the half-light times. Adapted from Elliot, Stansberry et al. (1997)

Thus by fitting this improved model to the IRTF Tr148B light curves, (Elliot, Stansberry et al. 1997) were able to directly fit for an ellipticity and position angle of the fit from a single light curve. The results of these fits are in Table II. The difference in the half-light radii given in Table II and those from the Tr148 astrometric solution given in Table I are attributed to the Olkin, Elliot et al. (1997) analysis reporting values in the shadow plane, which due to refraction are one scale height smaller than values at the planet as reported by Elliot, Stansberry et al. (1997).

Because of the inherent ambiguity of the orientation of the ellipse when fitting to only one light curve, (Elliot, Stansberry et al. 1997) fit for both an oblate and prolate solution (actually, two elliptical cross-section with a 90 degree uncertainty) to the atmospheric half-light figure. Given in Table II are the probabilities of fits with those parameters resulting from random noise superimposed on a circular figure (assuming the residual levels from the fits themselves). While the prolate model could be expected from a circular figure with noise about one time in ten, the oblate model, a more intuitively physical solution in any case, is hard pressed to have resulted from

a circular figure distorted by noise illustrated by the probability of only 5.5 x 10^{-7}, a very small chance indeed.

Table II: Atmospheric Figures from the Tr148B Central-Flash Analysis[a]

	Prolate Fit	Oblate Fit
Equatorial Half-light Radius[b] (km)	1441.4 ± 2.3	1450.8 ± 1.9
Ellipticity	0.014 ± 0.003	0.018 ± 0.003
Position Angle[c] (deg)	93.7 ± 6.4	2.5 ± 5.2
F-Test Probability[d]	9.9 x 10^{-2}	5.5 x 10^{-7}

[a] (Elliot, Stansberry et al. 1997).

[b] For the oblate fit, the semi-major axis is given, while for the prolate fit, the semi-minor axis is given.

[c] Pole position of the semi-minor axis measured from North through East.

[d] The probability that this fit would result from a truly circular figure plus random noise assuming the residuals of the fit.

Note from Table I and Table II that even though both methods of reducing the Tr148 occultation data set result in measurable ellipticities, the magnitude and orientation of these ellipses are not consistent for the two methods. The one sigma error bars of the occultation half-light solution include the solution calculated from the central flash, but the central-flash solution has much lower formal error, placing it better than two sigma away from the former. This is likely due to the small magnitude, as even slight errors can quickly skew the position angle of an ellipse. With the astrometric solution not inconsistent with a spherical atmosphere, and the central flash solution showing a clear tendency towards ellipticity but of a different magnitude and direction that the astrometric data, we continue looking for more information about Triton's atmospheric figure. Though it should be noted that the two methods are indeed probing different levels of the atmosphere. The half-light radius probed by the first solution is several scale heights above the area directly influencing the ellipticity determined from the central flash. Thus the variation in ellipticities could be a real effect related to this discrepancy.

Tr176 Astrometric Solution

The next good candidate for an occultation by Triton occurred in 1997. Also originally identified by McDonald and Elliot (1995), Tr176 was occulted by Triton on July 18, 1997. As the only good candidate since the Tr148 occultation, and having seen the importance of central flash data from the Tr148B IRTF light curves, the Tr176 event was proceeded by a massive prediction effort utilizing all available astrometry data in an attempt to pin down the viable central flash region and position a portable system in that area. Unfortunately, while the occultation was visible from both Australia and North America the portable stations that were set up in the central flash region on both continents (Tracones in Mexico, and Coen in Australia) acquired no data due to cloud cover (Elliot, Person et al. 2000).

Occultation light curves were obtained by Elliot, Person et al. (2000) from Chillagoe, Queensland and Brownsville, Texas, both using portable 14-in telescopes equipped with Portable CCD (PCCD) cameras (Buie, Millis et al. 1993; Dunham 1995), though these stations were both outside of the strong central-flash region. These two light curves were combined with three more (all taken in Australia) from another group (Sicardy, Mousis et al. 1998), also from outside the central-flash region.

An analysis based upon the Tr148 astrometric reduction (Olkin, Elliot et al. 1997) was performed upon the light curves with two minor differences. First, the central portion of the light curves were all retained as none of the five curves showed enough of a central flash to merit discarding asymmetric data.

Second, the least squares fitting routine for the atmospheric half-light figure was improved. In the Tr148 reduction, residuals in the timing differences of the half-light data points to the modeled figure were calculated along the vector from the center of the fitted figure through the data point, and were then corrected to the direction of travel of the occultation by multiplying by the appropriate cosine factor given the offset of the closest approach chord for that station from the center of the figure. This correction was done since the vast majority of the error in any data point is dominated by the error in the half-light time rather than the observer position. Small errors in the

coordinates of the station or Triton's ephemeris that could result in errors perpendicular to the chord are dwarfed by the timing accuracy along the chord. In the Tr176 astrometric fits, the residuals being minimized were all calculated in distance (multiplying the times by the occultation velocity) starting at the data points and measured directly along the paths of the shadows chords from data point to the fitted figure.

Figure IV displays the resulting plot of the half-light points as related to the Triton figure. The dotted and solid figures represent the best fitted elliptical and circular solutions to the half-light figure respectively. Table III gives the parameters for the half-light figures resulting from these fits. Here again, half-light radii are given in the shadow plane. In this case the differences between these values and those given by (Olkin, Elliot et al. 1997) and reported in Table I are real and are presumed to be due to increasing bulk in Triton's atmosphere over the intervening years between the occultations (Elliot, Hammel et al. 1998; Elliot, Strobel el at. 2000; Elliot, Person et al. 2000).

Figure IV: Tr176 Astrometric Solution

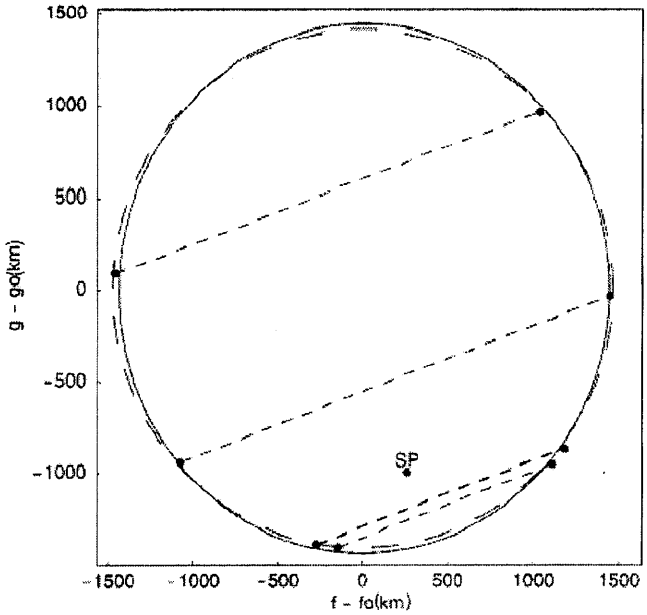

Figure IV: *Tr176 occultation geometry.* All five chords of the Tr176 occultation are plotted over the best fitting models of the atmospheric figure. The solid line is the best fitting circular model and the dotted line is the best fitting elliptical model. The point marked "SP" is the south pole of Triton. Note that the data points more cleanly align with the elliptical model. Adapted from Elliot, Person et al. (2000)

Note once again that the elliptical fit results in a much cleaner agreement with the data points as seen in both Figure IV and the RMS errors given in Table III. Though this elliptical fit seems to be in agreement in magnitude with the Tr148 astrometric reduction given in Table I, again the position angle of the ellipse is uncertain, and different from those given previously.

Table III: Atmospheric Figures from Tr176 Half-Light Analysis[a]

	Circular Fit	Elliptical Fit
Half-light Radius[b] (km)	1439 ± 10	1439 ± 7
Ellipticity	N/A	0.040 ± 0.003
Position Angle[c] (deg)	N/A	30 ± 5
Weighted RMS Error (km)	21.1	3.4

[a] (Elliot, Person et al. 2000)

[b] For the elliptical fit, the semi-major axis is given in the shadow plane, which is one scale height smaller than the radius at the planet due to refraction by the atmospher.

[c] Pole position of the semi-minor axis measured from North through East.

New Reduction of Tr148 Half-Light Solution

Tr148 FOS Analysis

As was mentioned in the previous chapter, the Tr148 astrometric solution could be improved, or at least have our confidence in it improved, if one could independently establish the separation and position angle between the two members of the double star system. In an attempt to establish this, MIT SB candidate Melissa Hayes reduced data taken of the binary system by Amanda Bosh with the HST Faint Object Spectrograph (FOS) on August 14, 1995, the day of the Tr148 event (Hayes 1996).

The FOS data were taken with a mirror instead of a grating, so in that mode the images are not dispersed, though they are elongated due to the optics of the spectrograph. But this effect can easily be accounted for in the analysis and individual point spread functions (PSF) can be fit to each of the star images. In this case, the image of the brighter star of the system (Tr148A) was used to define the PSF. This numerical PSF was then fit to the image of Tr148B to locate its position with respect to Tr148A.

The primary difficulty in this analysis procedure is calibrating the plate scale of the FOS detector. Two coordinate description matricies provided in the headers from the image files indicated that the instrument plate scale in the x and y directions were not consistent with the values measured from separate astrometric reductions (Hayes 1996).

Hayes identified a possible source of error in this method as the repeatability and consistency of the stepping and shifting of the image across the virtual pixels of the detector. Analysis of this effect by Lyons (1993) at the 1993 HST Calibration Workshop indicates that there may be significant error in each sub-step shift of the data on the detector.

Given these conclusions, the FOS data was used to produce updated astrometric solutions for the Tr148 occultation as a comparison (presented in Table V), but confidence in the results are

much higher for the following Fine Guidance System (FGS) analysis than those generated with the Faint Object Spectrograph.

Tr148 FGS Analysis

Hoping to resolve the discrepancy between the Tr148 half-light and central flash solutions, another instrument of the HST, the Fine Guidance System, was used by Elliot, Wasserman, and Franz to make an independent measurement of the positions of the two constituents of the Tr148 double star system.

Analyzing several FGS scans across the system on each of three dates in 1997 and 1998, Wasserman reduced the individual interference fringes recorded by the FGS and disentangle the separate positions of Tr148A and Tr148B. Producing a weighted average of the results from each of the three nights, Wasserman produced a list of FGS separations and position angles for the double star system.

The absolute orientation of these position angles depends upon the roll angle of the HST. This angle is recorded for each scan in the variable ROLLV3 in the header information of the scan data file. Unfortunately, this value is only the intended value the telescope is aiming for under the control of its positioning gyroscopes and fixed head star trackers. This value is often slightly different from the value determined by the Observatory Monitoring System (OMS) after the fact. The OMS value is calculated from the later analyzed locations of the guide stars in the guiding FGS's and their coordinates. Thus the accuracy of the OMS value itself is dependent upon the accuracy of the positions of the guide stars. The Space Telescope Science Institute FGS Instrument Handbook indicates that the error on this computed value due to guide star positioning is 0.04 degrees (Nelan and Makidon 1999).

The original analysis by Wasserman of the FGS scans used the roll angle reported in the ROLLV3 variable rather than the later reported OMS value. As the 0.04 deg expected error on the OMS roll angle is much less than the 0.4 deg error expected on the ROLLV3 value, the OMS values for the scans were retrieved from the Hubble Space Telescope Data Archive (STSCI 2001).

The difference between these OMS values and the ROLLV3 values were applied as a correction to the rotation of the field to adjust the position angles measured by Wasserman. The OMS values and the correction to the position angles appear in Table IV. The corrected values from Table IV were subtracted from Wasserman's values in calculating the position angles given in Table V.

Table IV: FGS Roll Angles and Corrections

FGS Scan Date	ROLLV3 (deg)	OMS Roll[a] Angle (deg)	Correction Angle (deg)
August 5, 1997	262.33	262.38	–0.05
November 7, 1997	259.95	260.29	–0.34
October 11, 1998	260.29	260.00	+0.29

[a] Retrieved from the HST Data Archive.

Note the disagreement between the FOS measurement and the three FGS measurements in Table V. Even the relatively large error estimated from the fits in the FOS reduction is insufficient to make up the difference. The FGS fits, while generally agreeing with each other and the original occultation fitted solutions, do scatter more than their formal errors would indicate.

Separation Trends

Given the lack of agreement between the three separate FGS measurements, considering their errors, it seems natural to search for a trend in the separation data. Such a trend would be expected if the two stars are part of a mutually orbiting system or if their relative proper motions were high enough to affect their separation over the time span of the observations. Figure V shows the scatter in the three measurements of the Tr148A-Tr148B separation from Table V.

Figure V: Tr148A-Tr148B Separation

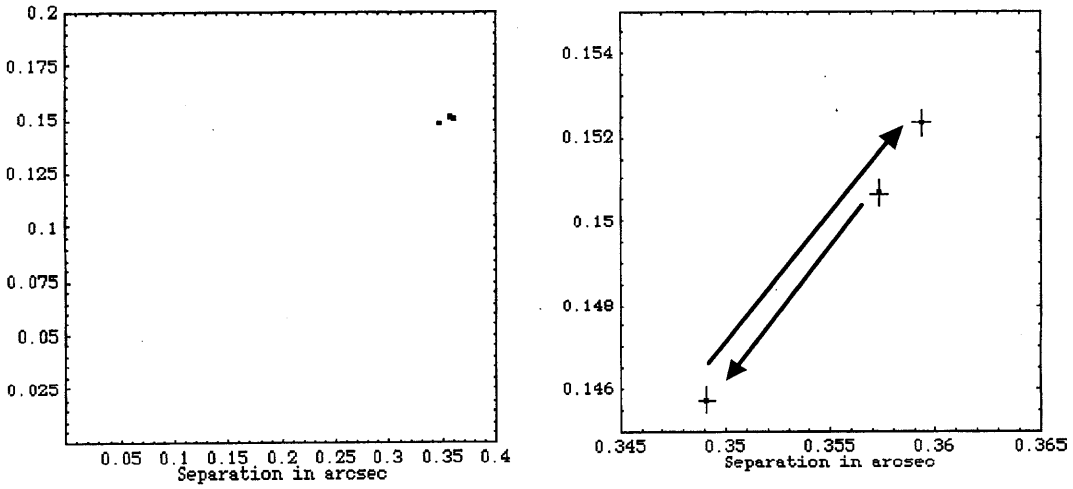

Figure V: *Tr148 Double Star Separation.* The left plot shows the separation in arcsec of Tr148B from Tr148A, for each of the three measurements made with the FGS. The right plot gives an expanded view of the region if interest, showing the errors on each point derived from those given in Table V. On both plots, North is plotted up, and East to the right. Note that in both plots the Y-axis has been compressed b y a factor of two. The arrows in the right side plot indicate the temporal sequence of the three points.

Plotting the three points versus time, in order to look for any temporal trends yields Figure VI.

Figure VI: Linear Trends in Separation Parameters

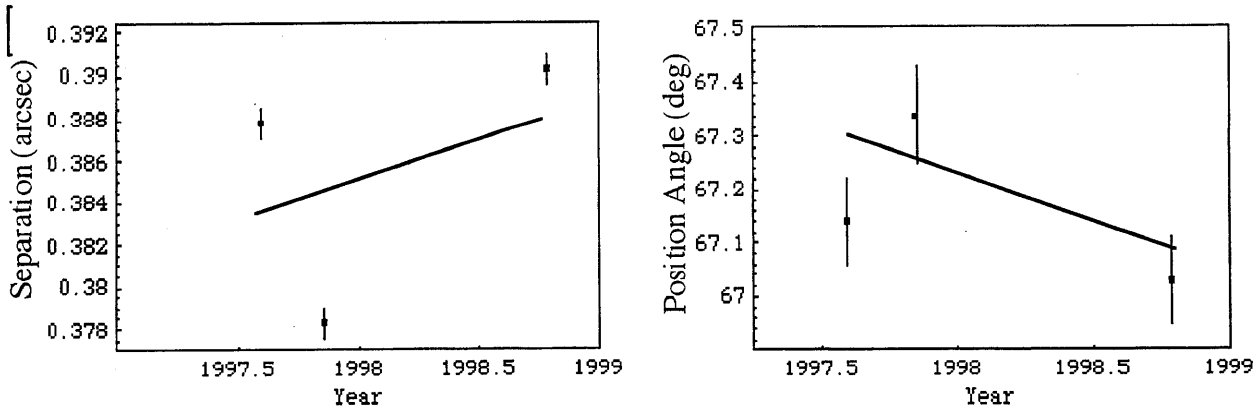

Figure VI: *Tr148 Double Star Separation Trends.* The plots show the three measurements of the Tr148A-Tr148B separation parameters (with error bars) with respect to time. Separation is plotted on the left, position angle is plotted on the right. The lines are the best fitting linear least square solutions through the points. The separation plot yields a linear correlation coefficient of 0.49, and the linear correlation coefficient for the position angle is 0.62.

Making a least squares linear fit to the three points from both graphs results in a trend in separation radius of 0.005 arcsec per year, and a trend in position angle of –0.156 degrees per year. As noted in the figure caption, the linear correlation coefficients for these two fits are low. Following the formalism of Bevington and Robinson (1992), the probability that two completely uncorrelated variables would have a linear correlation coefficient higher than those calculated for the fits is 72% for the separation radius fit and 59% for the position angle fit. Thus, there is little confidence in any systematic trend from these data. However, if the linear trend is accepted from the two plots, extrapolating this solution back to the time of the Tr148 event yields a "corrected" separation radius of 0.3731 ± 0.0011 arcsec with a position angle of 67.55 ± 0.11 deg.

Disregarding the trends and considering the three FGS points as a single weighted average, we find a result of 0.3855 ± 0.0004 arcsec for the separation and 67.17 ± 0.05 deg for the position angle. While the errors in the separation are consistent with the magnitudes of the errors on the position angles, examination of the left hand plot of Figure VI indicates that these errors may be underestimated since their scatter about the fitted line is much greater than the error bars indicate. The error bar for the position angle in the right hand plot of Figure VI are generally in line with their scatter about the fitted line. Note that these calculated formal errors (especially for the separation) are significantly smaller than that error indicated from the scatter. Using only the scatter of the three points in each case, the errors on the means would be 0.0036 in separation and 0.09 in position angle.

The astrometric separation solutions from these analyses (trend extrapolation and averaging) are also given in Table V.

Table V: Measurements of the Tr148 Double Star System

Date/Solution	Method	Tr148A/Tr148B Separation (arcsec)	Position Angle[a] (deg)
August 14, 1995	FOS	0.3652 ± 0.0036	69.45 ± 0.25
August 14, 1995 (Table I)	Half-Light Fit	0.3874 ± 0.0011	65.16 ± 0.14
August 14, 1995	Half-Light Fit[b]	0.3869 ± 0.0009	66.02 ± 0.11
August 5, 1997	FGS[c]	0.3878 ± 0.0007	67.14 ± 0.08[d]
November 7, 1997	FGS[c]	0.3783 ± 0.0007	67.34 ± 0.08[d]
October 11, 1998	FGS[c]	0.3903 ± 0.0007	67.03 ± 0.09[d]
Averaged FGS Solution	FGS	0.3855 ± 0.0004[e]	67.17 ± 0.05[d,e]
Extrapolated FGS Solution[f]	FGS	0.3731 ± 0.0011[e]	67.55 ± 0.11[d,e]

[a] Position angle of Tr148B with respect to Tr148A, measured North through East.

[b] This is the original data set on the line above, but refit using the improved routines discusses in the *Tr176 Astrometric Solution* section.

[c] FGS position angles are modified by the correction factors given in Table IV.

[d] The given position angle errors do not include the 0.04 degree random error due to guide star position errors. (Nelan and Makidon 1999).

[e] These errors are based upon the formal errors calculated from the FGS solution. Errors based upon the scatter of the various FGS points would be similar in position angle, but about three times higher in separation.

[f] FGS trends in separation and position angle (described in previous section) extrapolated back to the occultation date (August 14,1995).

Refitting for Triton's Atmospheric Figure

Given the these various means of finding an independent measurement of the Tr148 separation, it was possible to refit the astrometric solution holding the Tr148A-Tr148B separation and position angle as fixed parameters instead of free in the fit. The improvement in how the residuals were calculated discussed in the *Tr176 astrometric solution* section of the previous chapter was also implemented in all the following fits. (The residuals minimized were parallel to the direction of the occultation chord paths instead of perpendiculars to the atmospheric half-light figure.)

Otherwise, fitting proceeded identically to the fitting procedure used in the original Tr148 astrometric solution by Olkin, Elliot et al. (1997). The new results (all oblate fits) are given in Table VI.

Table VI: Triton Atmospheric Figure Solutions

Method for Determing Double Star Separation	Atmospheric Ellipticity	Pole Position Angle[a] (deg)	Reduced Chi-Squared	Probability[b]
Circular Fit[c,d]	0.000	N/A	2.1	5%
Elliptical Fit[c,d]	0.029 ± 0.016	70.3 ± 10.1	1.7	14%
Occultation Fit Recalculated[d,e]	0.030 ± 0.015	68.2 ± 9.9	1.6	18%
Averaged FGS[f]	0.033 ± 0.013	65.1 ± 8.8	1.1	38%
Extrapolated FGS[g]	0.038 ± 0.019	52.1 ± 11.4	1.9	9%
FOS	0.041 ± 0.023	47.8 ± 14.1	2.2	3%
Pole Position Angle Fixed[h]	0.043 ± 0.026	2.5	2.1	5%

[a] Position angle of the semi-minor axis measured from North through East.

b The probability that data with random Gaussian noise, fitted to a model that correctly describes the distribution, would have a reduced chi-squared value higher than the value given.

[c] (Olkin, Elliot et al. 1997)

[d] These fits allowed the separation and the position angle of the Tr148 double star to be free parameters in the fits.

[e] Original (Olkin, Elliot et al. 1997) solution (previous table line) re-analyzed through the improved Tr176 code discussed in the previous chapter. .

[f] Tr148 separation parameters were fixed at the weighted average of all three FGS measurements. (From Table V)

[g] Tr148 separation parameters were fixed at the extrapolated FGS solution given in Table V.

[h] Pole position angle fixed at the value determined from the Tr148 central flash solution. (Table II).

The figure derived from the FGS measurements exhibits a lower reduced chi-squared than the similar Tr148 astrometric elliptical fit, and thus provide a greater confidence in the non-sphericity of Triton's atmosphere. Also, note that it also has a lower reduced chi-squared value than the best Tr148 circular solution by almost a factor of two.

One final solution, given in the final line of Table V, is a free fit to the occultations chords (similar to the "Occultation Fit Recalculated" solution), in which the position angle of the ellipse was fixed to that value determined from the Tr148 central flash solution. This fit is labeled "Pole Position Angle Fixed".

Compilation and Analysis

Table VII has a compiled list of ellipticities and position angles from the occultation reductions presented in previous chapters. Due to the uncertainties associated with the FOS reduction, this solution was dropped from the final list. Also dropped is the FGS extrapolated solution, due to low confidence in the fits to the linear trends noted previously.

Table VII: Compiled Triton Half-Light Ellipticity Parameters

	Ellipticity	Position Angle[a]	Triton Pole[b]
Tr148 Half-Light Solution[c]	0.029 ± 0.016	70.3 ± 10.1	3.2
Tr148 Half-Light Solution Recalculated[d]	0.030 ± 0.015	68.2 ± 9.9	3.2
Averaged FGS[e]	0.033 ± 0.013	65.1 ± 8.8	3.2
Tr148 central flash	0.018 ± 0.003	2.5 ± 5.2	3.2
Tr176 Half-Light Solution	0.040 ± 0.003	30 ± 5	–4.1

[a] Position angle of the semi-minor axis measured from North through East.

[b] Pole position angle of Triton measured North through East.

[c] Olkin, Elliot et al. (1997)

[d] This work. Original (Olkin, Elliot et al. 1997) solution (previous table line) re-analyzed through the improved Tr176 code discussed in the previous chapter.

[e] Tr148 separation parameters were fixed at the weighted average of all three FGS measurements. (From Table V)

As seen in Tables V and VI, the astrometric fits to the ellipticity of Triton's half-light figure all agree to within two sigma of each other. The fitted ellipticities vary from approximately 0.03 to approximately 0.04 and the position angles vary within 10 degrees of 60.0. The sole exception to this is the position angle of the Tr176 astrometric fit, but as this data set has a much lower signal to noise level than the Tr148 occultation, this is not necessarily a refutation. A second difference that could lead to this discrepancy is that Triton's actual pole position angle varied by 7.3 degrees between the two events with a value of 3.2 for the Tr148 event and –4.1 for the Tr176 event. This difference compares to about one sigma errors on the fitted atmospheric position angles and may

help to explain the discrepancies between the half-light solutions. Applying the correction to the Tr176 half-light solution brings the two solutions to within 2.5 sigma of each other.

The improved Tr148 solution calculated in this work continues to not agree with that of the Tr148 central flash data. Even forcing the position angle of the astrometric fits to the Tr148 value produces unacceptable fits, as shown in the previous chapter.

This discrepancy need not be treated too strongly, however, as the two methods involved could simply be indicating a complicated atmospheric structure. The central flash solution, generated by fitting a light curve to determine the shape of the central evolute is probing the atmosphere several scale heights below the half-light level, which is the level that is driving all of the atmospheric solutions. Indeed if we assume that the atmospheric figure must be nearly circular (maximum ellipticity of 0.002 ± 0.001) at the surface, given the firm constraints on non-sphericity in the body (Thomas 2000), it is reasonable to assume as a first approximation at points in between the surface and the half-light level, the shape of the atmospheric profile will continuously decrease in ellipticity from its half-light value to zero at the surface. Seen in this light, it is perhaps not inconsistent that the central flash ellipticity is lower than that measured by the astrometric half-light solutions.

The inconsistencies in the position angles of the various reductions are more difficult to reconcile in this way and may hint at a more complicated three-dimensional structure beyond a simple ellipsoid in projection.

Discussion

Sources of Ellipticity

Having determined that some non-sphericity clearly exists in the atmosphere, it is instructive to examine the possible sources and the problems with each.

As mentioned in the introduction, Voyager 2 images of the limbs of Triton were reduced by Thomas (2000) indicating that the solid surface of Triton has almost no ellipticity, with an upper limit over 30 times smaller than the Elliot, Stansberry et al. (1997) Tr148 central flash measurements. This would indicate that any ellipticity exhibited by the atmosphere must be solely the result of atmospheric processes. A severely asymmetric internal mass capable of raising the atmospheric figure would result in a harmonic mass distribution coefficient (J_2) as high as 0.06, a value inconsistent with the apparent relaxed shape of the body ($J_2 < 10^{-4}$) indicating that atmospheric distortions are not due to physical body distortions (Thomas 2000).

The obvious alternative then is a constant significant equatorial wind, or at least one perpendicular to the pole of the ellipse measured. The difficulty with this theory is that given low J_2 gravitational distortion implied by the near spherical surface, the ellipticities given by the larger measurements in Table VII imply a sustained wind speed of over 280 m/s. This is twice the sonic velocity of only 140 m/s at this pressure (Elliot, Stansberry et al. 1997; Elliot, Person et al. 2000).

Though the speeds are smaller than those calculated to support the ellipticity, there are several indications of strong winds on Triton. Voyager 2 images indicate clear wind streaks on the surface (Hansen, McEwen et al. 1990) and stereograph image comparison indicates horizontal shearing of a rising plume in the atmosphere (Soderblom, Kieffer et al. 1990). Thus some winds seem to exist on Triton if not as large as those needed to cause the observed ellipticity.

Elliot, *et al.*'s (Elliot, Stansberry et al. 1997; Elliot, Hammel et al. 1998; Elliot, Person et al. 2000) observations of increasing atmospheric pressure indicate that significant changes are occurring on Triton at the moment. If the observed winds are responsible for a portion of the

ellipticity observed, processes associated with the increasing pressure (such as asymmetric outgassing of the surface ice) could conceivably result in the remainder.

Conclusions

Stellar occultations provide our only current means of monitoring the actual shape of the atmosphere for a body so far and small as Triton. Over the three years from 1995 through 1997, three occultations Tr148, Tr176, and Tr180, were observed with sufficient assets to produce a measurement of the projected ellipticity of the two-dimensional half-light figure of the atmosphere. The fact that all current analyses of these events results in a significant ellipticity, at times reaching as high as 4%, indicates that Triton's atmosphere is significantly distorted from a symmetric sphere. After improving the reduction of the Tr148 solutions as much as possible, by including all currently available data and more recent reduction techniques, the ellipticity measured seems consistent (within two sigma) with other measurements (Tr148 central flash, Tr176 half-light solution). Accounting for the change in Triton's pole position angle between the two events, the position angles of the elliptical solutions agree to within 2.5 σ. This gives a firm indication that the presumed non-sphericity is indeed real, though the differences in the measurements tell us that further monitoring of the situation is needed.

Assuming that there is a non-sphericity as large as those measured, it is unclear what processes can be supporting it. Given the almost total absence of an ellipsoidal shape to the body itself, it seems that any non-sphericity must be supported by solely atmospheric processes, but those known are not strong enough to support the ellipticities measured from the occultation data sets. Further data is needed to both monitor and confirm this non-sphericity, and occultations remain the only means of measuring the phenomenon currently available, so effort directed at observing future Triton occultations is encouraged. McDonald and Elliot (2000) predict several such occultations over the next decade, including Tr231 in August of 2001, the next most likely candidate to be observed.

Ideally, these observations and future one would be combined with more robust modeling of the three dimensional processes in the atmosphere to gain a better understanding than is currently possible of the full picture.

Acknowledgements

I would like to thank Professor James L. Elliot, MIT, and the members of the MIT Planetary Astronomy Lab for all of their continuing encouragement and advice.

I would also like to thank Dr. Larry Wasserman, Lowell Observatory, for all of his excellent work in reducing the Tr148 FGS scans, and Otto Franz of Lowell Observatory for his work in planning the HST FGS observations.

This work was funded in part by the Space Telescope Science Institute (Grants GO-07489 and GO-07490) and the National Aeronautics and Space Administration (Grant NAG5-3940).

References

Baum, W. A. and A. D. Code (1953). "A photometric observation of the occultation of σ Arietis by Jupiter." Astronomical Journal **58**: 108-112.

Bevington, P. R. (1969). Data Reduction and Error Analysis for the Physical Sciences. New York, McGraw-Hill Book Company.

Bevington, P. R. and D. K. Robinson (1992). Data Reduction and Error Analysis for the Physical Sciences. New York, McGraw-Hill Inc.

Buie, M. W., R. L. Millis, et al. (1993). "CCD Camera Occultation System." Bulletin of the American Astronomical Society **25**(3): 1115.

Dunham, E. W. (1995). Optical instrumentation for airborne astronomy. Proceedings of the Airborne Astronomy Symposium on the Galactic Ecosystem: From Gas to Stars to Dust. M. R. Haas, J. A. Davidson and E. F. Erickson. San Francisco, ASP**:** 517-522.

Elliot, J. L., A. S. Bosh, et al. (1993). "An occultation by Saturn's rings on 1991 October 2-3 observed with the Hubble Space Telescope." Astronomical Journal **106**(6): 2544-2572.

Elliot, J. L., H. B. Hammel, et al. (1998). "Global warming on Triton." Nature **393**(6687): 765-767.

Elliot, J. L., M. J. Person, et al. (2000). "The prediction and observation of the 1997 July 18 stellar occultation by Triton: More evidence for distortion and increasing pressure in Triton's atmosphere." Icarus **148**(2): 347-369.

Elliot, J. L., J. A. Stansberry, et al. (1997). "Triton's distorted atmosphere." Science **278**: 436-439.

Elliot, J. L. and L. A. Young (1992). "Analysis of stellar occultation data for planetary atmospheres. I. Model fitting, with application to Pluto." Astronomical Journal **103**(3): 991-1015.

Hansen, C. J., A. S. McEwen, et al. (1990). "Surface and airborne evidence for plumes and winds in Triton." Science **250**: 421-424.

Hansen, C. J. and D. A. Paige (1992). "A thermal model for the seasonal nitrogen cycle on Triton." Icarus **99**(2): 273-288.

Hayes, M. N. (1996). Separation of a Double Star from Hubble Faint Object Spectrograph Data. Department of Physics. Cambridge, Massachusetts Institute of Technology: 49.

Institute, S. T. S. (2001). HST Data Archive, Association of Universities for Research in Astronomy. **2001**.

Lyons, R. W. (1993). Position Repeatability of Spectra Obtained with the FOS. HST Calibration Workshop.

McDonald, S. W. and J. L. Elliot (1992). "Triton stellar occultation candidates: 1992-1994." Astronomical Journal **104**: 862-879.

McDonald, S. W. and J. L. Elliot (1995). "Triton stellar occultation candidates: 1995-1999." Astronomical Journal **109**: 1352-1362.

McDonald, S. W. and J. L. Elliot (2000). "Triton stellar occultation candidates: 2000-2009." Astronomical Journal **119**: 936-944.

Nelan, E. P. and R. B. Makidon (1999). Fine Guidance Sensor Instrument Handbook. Baltimore, MD, Space Telescope Science Institute.

Olkin, C. B., J. L. Elliot, et al. (1997). "The thermal structure of Triton's atmosphere: Results from the 1993 and 1995 occultations." Icarus **129**: 178-201.

Sicardy, B., O. Mousis, et al. (1998). "Structure of Triton's atmosphere from the occultation of Tr176." Bulletin of the American Astronomical Society **30**(3): 1107.

Smith, B. A., L. A. Soderblom, et al. (1989). "Voyager 2 at Neptune: Imaging science results." Science **246**: 1422-1449.

Soderblom, L. A., S. W. Kieffer, et al. (1990). "Triton's geyser-like plumes: Discovery and basic characterization." Science **250**: 410-415.

Spencer, J. R. (1990). "Nitrogen frost migration on Triton: a historical model." Geophysical Research Letters **17**(10): 1769-1772.

Strobel, D. F., X. Zhu, et al. (1996). "On the vertical thermal structure of Pluto's atmosphere." Icarus **120**(2): 266-289.

Thomas, P. C. (2000). "The Shape of Triton from Limb Profiles." Icarus **148**: 587-588.

Appendix A: Calculation Notebooks and Files

This appendix lists all of the Mathematica™, Kaleidagraph™ and Excel™ files used in generating results in this work. For each table the files use to generate the results contained therein are listed. These files are all stored on the MIT Planetary Astronomy Lab machine lowell.mit.edu in the folders labled "LOWELL:Local Files: Projects: Triton:Tr148:", "LOWELL:Local Files: Projects: Triton:Tr176:", and "LOWELL:Local Files:Theses:Person 2001".

Table A: Calculation Sources

Thesis Table	Notebooks and Files
Table I	Tr148AB_ellipse9_1.3.nb
Table II	Asymmetry_Note_calc_1.3.m
	CF_Light_Curve_1.9.m
Table III	Tr176 ellipse fits 1.8.nb
	Tr176 Paper I Calcs 2.4.nb
Table IV	Person_Thesis_calcs.1.8.nb
Table V	HST separation 1.0.w
	Person_Thesis_calcs.1.8.nb
	separations figure 1.0.nb
	separation graphs 1.0.kgd
Table VI	Tr176 ellipse fits 1.8.nb
	Thesis ellipse fits 2.1.nb